A Comparative Analysis of Solar-Assisted ORC and Refrigeration System for Supercritical Working Fluids

Onder Kizilkan and Hiroshi Yamaguchi

Abstract In present study, a comparative thermodynamic assessment of a solar-driven organic Rankine cycle integrated with an absorption refrigeration system was performed. During the analyses, parabolic trough solar collectors were used to meet the necessary thermal energy for the power and refrigeration cycles. For the absorption refrigeration, the H_2O-LiBr cycle was proposed for the integrated system in order to maintain chilled water. The analysis was carried out for three supercritical working fluids: carbon dioxide (R744), ethane (R170), and fluoromethane (R41). For specified parabolic trough collector parameters, energetic and exergetic performances of the cycles were determined for constant turbine inlet pressure and constant pressure ratio. A parametrical study was also implemented for determining the effect of the system parameters on cycle performances. According to the results, the best performance was achieved using R41 with a net energy production rate of 32.54 kW, followed by R170 and R744. Based on the results of the exergy analysis, the leading exergy destruction rate was estimated for the integrated cycle working with R744. Additionally, the necessary collector length and area were determined for specific net power generation and refrigeration duties.

Keywords Organic Rankine cycle · Supercritical fluid · PTSC · Absorption refrigeration

1 Introduction

In the past several decades, a great amount of the world's power generation requirement is satisfied by facilities that are based on fossil fuels. On the other hand, the

O. Kizilkan (✉)
Department of Mechanical Engineering, Faculty of Technology, Isparta University of Applied Sciences, 32200 Isparta, Turkey
e-mail: onderkizilkan@isparta.edu.tr

H. Yamaguchi
Department of Mechanical Engineering, Doshisha University, Kyo-Tanabeshi, Kyoto 610-0321, Japan

© The Author(s), under exclusive license to Springer Nature Singapore Pte Ltd. 2023

V. Edwin Geo and F. Aloui (eds.), *Energy and Exergy for Sustainable and Clean Environment, Volume 2*, Green Energy and Technology,
https://doi.org/10.1007/978-981-16-8274-2_32

excavated fossil-based fuels are utilized for generating heat energy or converted into practical industrial equipment. Due to the fact that these resources are being depleted, exhausting fossil-based fuels give rise to a severe energy crisis. Accordingly, sustainable and clean energy resources that are renewable and more environmentally friendly to substitute fossil fuels are being pursued by many investigators and industrial sectors [1]. Within renewable resources, solar thermal energy certainly has the greatest potential. When the environmental costs are taken into account, solar energy can be financially competitive with fossil fuel-based electricity generation. However, without taking into account such environmental costs, solar-based energy generation systems are not cost competitive currently due to the high capital investments. On the other hand, it is possible to reduce the investment costs by improving the performance of solar thermal power systems [2]. Among the solar thermal applications, parabolic trough solar collectors regarded as the most developed technology for electricity generation from solar thermal power [3]. This kind of collectors has been utilized in bigger power plants for the last four decades, exhibiting a promising future [4].

One of the major ways to generate energy from low and medium-temperature energy resources, such as solar energy, is utilizing the organic Rankine cycle (ORC). Although it has got many advantages, the major problem of these kinds of power plants is the relatively lower energy efficiency. A possible solution for increasing the energy production efficiency of the Rankine cycle may be the utilization of supercritical working fluid in order to create a supercritical cycle, which is widely known and has been implemented satisfactorily in a wide range of applications [5].

Supercritical natural fluids are becoming the most promising working fluids, especially in low-temperature power generation with organic Rankine cycles (ORCs). Among these, carbon dioxide (CO_2), as a supercritical fluid, has received increasing attention in low-temperature power generation applications of Rankine cycles for the last decades [6–8]. As an environmentally benign working fluid, without ozone depletion potential and insignificant global warming potential, CO_2 is non-flammable, poisonous, and inexpensive, which is a naturally occurring substance and abundant in the atmosphere. In addition, the heat transfer properties of CO_2 are quite satisfactory, and the specific volume of CO_2 is reasonably lower, which leads to a reduction in the component dimensions for the same operational states. On the other hand, there two major problems appear during the operation of the CO_2 cycles. The first one is the operating pressure which is relatively higher when compared to the other cycles, and the second one is the somewhat lower efficiency [9]. One of the other proper working fluids to be utilized in a supercritical cycle is possibly ethane (R170) due to its lower critical temperature and pressure. However, one crucial drawback of ethane as a working fluid is its cracking and chemical decomposition at high temperatures. Ethane is utilized as a refrigerant at low temperatures, while it is cracked to produce ethylene at high temperatures [10]. Another working fluid with lower critical properties such as CO_2 is fluoromethane (R41). R41 is a non-toxic, liquefiable, and flammable gas at reference conditions, but its ignition lower limit is high. Since it does not contain chlorine, it is not destructive to the ozone layer. Thus, owing to its properties, it can be used in supercritical cycles likewise [11].

Air conditioning demands occur mainly during summertime when the solar radiation is very high, and this facilitates generating electric power along with cooling utilizing the solar thermal energy [12]. A solar-powered absorption refrigeration system is one of the most common ways of utilizing solar energy [13]. Today, water–lithium bromide (H_2O-LiBr) is the most common working fluid commercially available for most industrial absorption systems. These systems serve for mainly air-conditioning applications [14].

In this study, a comparative thermodynamic analysis is carried out for evaluating the performance of the parabolic trough solar collector-based (PTSC) ORC integrated with the absorption refrigeration system. The proposed system is powered by solar energy using PTSC. For the ORC, three different supercritical working fluids are used for performance comparison, which are CO_2 (R744), ethane, and fluoromethane. For refrigeration purposes, an absorption refrigeration system (ARS) working with H_2O-LiBr is integrated into the system. Additionally, exergy analysis is carried out in order to determine the exergy destructions.

2 Integrated Power and Refrigeration System

The schematic representation of the PTSC-based ORC integrated with the vapor absorption refrigeration cycle is shown in Fig. 1. Referring to Fig. 1, there are four sub-cycles, PTSC, ORC, ARS, and cooling tower (CT) cycle. In the PTSC cycle, the heat transfer fluid (HTF) enters the pump and is pumped to the PTSC field. While the HTF passes through the PTSC, it is heated up and enters to the vaporizer of ORC, where it gives some amount of its thermal energy to the working fluid. After passing the vaporizer, HTF enters the generator of ARS, and it gives the rest of its energy to

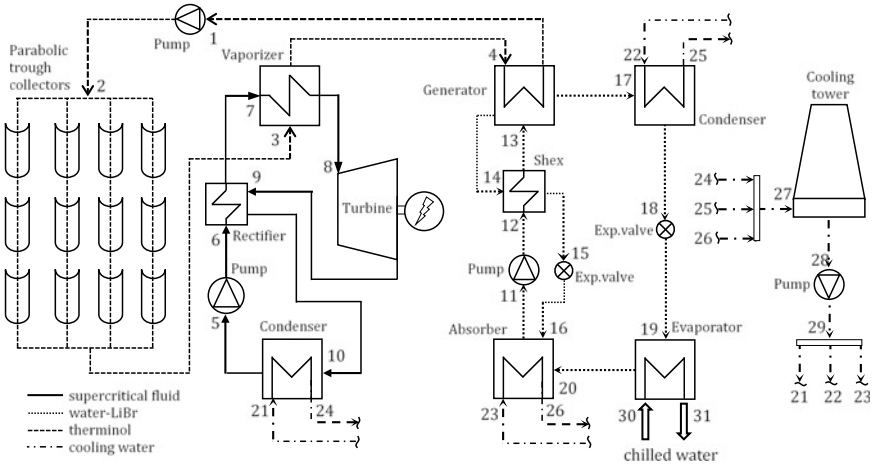

Fig. 1 Schematic representation of the PTSC-assisted ORC-ARS

the H_2O-LiBr couple. The ORC system consists of a turbine, a vaporizer, a condenser, a rectifier, and a pump. The superheated vapor needs to be cooled to a saturated liquid before entering the feed pump. In ORC, the saturated fluid is pumped to the rectifier, where it is preheated before the vaporizer. In the vaporizer, it reaches a supercritical temperature and pressure and enters the turbine. While passing through the turbine, some amount of thermal energy of the working fluid is converted to mechanical energy, and it exits the turbine with lower pressure. After, it enters the condenser, where it becomes a saturated liquid and pumped again by the feed pump. The ARS is working with the H_2O-LiBr couple. The fluid pair is pumped by the feed pump of ARS and enters the generator after preheated by the solution heat exchanger (Shex). In the generator, the fluid pair is heated up, and due to low pressure, some amount of water evaporates below 100 °C. The vapor water then enters the condenser, becomes saturated liquid, passes from the expansion valve, while its pressure is decreased and enters the evaporator. In the evaporator, the water becomes saturated vapor under very low pressure, while it cools down the coolant water for air-conditioning purposes. After exiting the evaporator, it reaches the absorber, and in the absorber, it is mixed with the fluid pair coming from the generator by rejecting some amount of heat. Additionally, the integrated system includes a CT system for absorbing the reject heat energy from the cycles. For the analysis, the main design parameters of the PTSC are given in Table 1.

Three supercritical fluids are selected for the performance analysis of the solar energy-driven ORC: R744, R170, and R41. These fluids were selected because of their low critical temperature and pressures. The working fluids with lower critical properties execute well for supercritical cycles, but the chemical stability of these kinds of working fluids utilized in supercritical cycles also relies on their critical properties, especially critical temperature due to the fact that with a high degree of superheat, they tend to degenerate [16]. As can be seen from Table 2, all three selected fluids have critical temperatures between 30 and 45 °C.

3 Methodology

In order to assess the thermodynamic performance of the solar energy-powered integrated system explained previously, energy and exergy analyses are performed. The assumptions listed below are made throughout the analyses:

- The system is in steady-state flow conditions.
- Kinetic and potential energies are ignored.
- No heat transfers from the heat exchangers and turbine to the environment.
- No pressure drops during the operation.
- The dead-state temperature T_0 is taken to be 20 °C, while the pressure P_0 is assumed as 101.325 kPa.

Table 1 General design x of the combined system [15]

PTSC	Inner diameter of receiver	0.08 m
	Outer diameter of receiver	0.09 m
	Outer diameter of cover	0.15 m
	PTSC length	100 m
	HTF mass flow rate	2 kg/s
	Emissivity of receiver	0.92
	Emissivity glass cover	0.87
	Temperature of the sun	5739 K
	Solar radiation	750 W/m^2
	Wind velocity	5 m/s
	Sun temperature	5739 K
ORC	Inlet pressure of turbine	9000 kPa
	Inlet temperature of turbine	140 °C
	Condenser temperature	25 °C
	Isentropic efficiency of turbine	0.88
	Isentropic efficiency of pump	0.92
ARS	Generator temperature	90 °C
	Condenser temperature	35 °C
	Absorber temperature	35 °C
	Evaporator temperature	5 °C
	Pump isentropic efficiency	0.95
	Shex effectiveness	0.83

Table 2 Properties of supercritical fluids studied [17]

	M (g/mol)	T_{bp} (°C)	T_c (°C)	P_c (MPa)	safety[1]	ALT[2]	ODP	GWP
R41	34.03	−78.12	44.13	5.8	NA	2.4	0	92
R170	30.07	−88.60	32.18	4.8	A3	0.21	0	~20
R744	44.01	−78.40	30.98	7.3	A1	>50	0	1

[1]ASHRAE 34 safety group
[2]Atmosphere life time

3.1 PTSC Modeling

In order to determine the solar energy amount absorbed by the parabolic trough collectors, the model given in Ref. [18] is used. The absorbed useful solar energy from the sun is determined by:

$$\dot{Q}_u = F_R[SA_a - A_r U_L(T_{in} - T_0)] \tag{1}$$

Here, S is the solar radiation; F_R is the heat removal factor; U_L is the heat loss coefficient of solar collector; A_a and A_r are collector aperture area and receiver area, respectively. The useful energy can also be calculated from:

$$\dot{Q}_u = \dot{m} c_p (T_{out} - T_{in}) \tag{2}$$

In Eq. (1), the heat removal factor F_R is described as:

$$F_R = \frac{\dot{m} C_p}{A_r U_L} \left[1 - \exp\left(\frac{-A_r U_L F'}{\dot{m} C_p} \right) \right] \tag{3}$$

In Eq. (3), F′ denotes the efficiency factor of collector and determined as:

$$F' = \frac{U_0}{U_L} \tag{4}$$

where U_0 represents the overall heat transfer coefficient. Since the receiver is encircled by an evacuated glass cover, the effects of convection heat transfer inside the receiver can be neglected. Thus, the heat loss coefficient can be calculated as:

$$U_L = \left[\frac{A_r}{\left(h_{c,c-a} + h_{r,c-a}\right) A_g} + \frac{1}{h_{r,r-c}} \right]^{-1} \tag{5}$$

In the above equation, $h_{c,c\text{-}a}$ is the heat convection heat coefficient between the glass cover and surroundings; $h_{r,c\text{-}a}$ is the radiation heat transfer coefficient between the glass cover and surroundings, and the radiation coefficient between receiver and glass cover is denoted by $h_{r,r-c}$. These coefficients are described below:

$$h_{c,c-a} = \frac{Nu_{air} k_{air}}{D_g} \tag{6}$$

$$h_{r,c-a} = \varepsilon_g \sigma \left(T_g + T_a\right)\left(T_g^2 + T_a^2\right) \tag{7}$$

$$h_{r,r-c} = \frac{\sigma \left(T_r + T_g\right)\left(T_r^2 + T_g^2\right)}{\frac{1}{\varepsilon_r} + \frac{A_r}{A_g}\left(\frac{1}{\varepsilon_g} - 1\right)} \tag{8}$$

In the above equations, k is the thermal conductivity; Nu is the Nusselt number; σ is Stefan–Boltzmann constant; ε is the emissivity. In addition, subscripts r and g represent glass cover and receiver, respectively. In Eq. (7), the Nusselt number is determined as a function of Reynolds number with the equations given below:

$$\mathrm{Nu}_{air} = 0.4 + 0.54\,\mathrm{Re}^{0.52} (0.1 < \mathrm{Re} < 1000) \tag{9a}$$

$$\mathrm{Nu}_{\mathrm{air}} = 0.3\ \mathrm{Re}^{0.6} (1000 < \mathrm{Re} < 50000) \tag{9b}$$

The temperature of glass cover T_{g} can be determined from the equation below:

$$T_{\mathrm{g}} = \frac{A_{\mathrm{r}} h_{\mathrm{r,r-c}} T_{\mathrm{r}} + A_{\mathrm{g}} \left(h_{\mathrm{r,c-a}} + h_{\mathrm{w}}\right) T_{\mathrm{a}}}{A_{\mathrm{r}} h_{\mathrm{r,r-c}} + A_{\mathrm{g}} \left(h_{\mathrm{r,c-a}} + h_{\mathrm{w}}\right)} \tag{10}$$

Finally, the overall heat transfer coefficient of the collector is determined by;

$$U_0 = \left[\frac{1}{U_{\mathrm{L}}} + \frac{D_{\mathrm{o}}}{h_{\mathrm{fi}} D_{\mathrm{i}}} + \left(\frac{D_{\mathrm{o}} \ln\left(\frac{D_{\mathrm{o}}}{D_{\mathrm{i}}}\right)}{2k} \right) \right]^{-1} \tag{11}$$

In the above equation, D represents diameter; h_{fi} denotes heat transfer coefficient of HTF flowing inside the pipes; subscripts i and o represent inner and outer, respectively. The convection heat transfer coefficient of the heat transfer fluid is calculated from the equation given below:

$$h_{\mathrm{fi}} = \frac{\mathrm{Nu}_{\mathrm{fi}} k_{\mathrm{fi}}}{D_{\mathrm{i}}} \tag{12}$$

$$\mathrm{Nu}_{\mathrm{fi}} = 0.023\ \mathrm{Re}^{0.8}\ \mathrm{Pr}^{04} (\mathrm{Re} > 2300) \tag{13a}$$

$$\mathrm{Nu}_{\mathrm{fi}} = 4.364 (\mathrm{Re} < 2300) \tag{13b}$$

3.2 Thermodynamic Modeling

The governing equations of mass and energy balance can be written as [19];

$$\sum \dot{m}_{\mathrm{in}} = \sum \dot{m}_{\mathrm{out}} \tag{14}$$

$$\sum (\dot{m} X)_{\mathrm{in}} = \sum (\dot{m} X)_{\mathrm{out}} \tag{15}$$

$$\sum \dot{E}_{\mathrm{in}} = \sum \dot{E}_{\mathrm{out}} \tag{16}$$

Here, $\dot{m}$ is the mass flow rate; $\dot{E}$ is the energy; subscripts in and out represent inlet and outlet streams, respectively. Moreover, X in Eq. (15) stands for the concentration ratio for the H_2O-LiBr cycle. The energy balance equation can be expressed more clearly as;

$$\dot{Q} + \sum \dot{m}_{\text{in}} h_{\text{in}} = \dot{W} + \sum \dot{m}_{\text{out}} h_{\text{out}} \tag{17}$$

where Q represents heat transfer, h is the enthalpy, and $\dot{W}$ is the work. In order to carry out thermodynamic modeling of vapor absorption cycle, the effectiveness method is used as a practical way of specifying the fluid temperatures entering and exiting the solution heat exchanger. If the effectiveness is known, other thermodynamic properties can be calculated from the definition of the heat exchanger effectiveness, which is given below [20];

$$\varepsilon = \frac{\dot{Q}_{\text{actual}}}{\dot{Q}_{\text{max}}} \tag{18}$$

In Eq. (18), the maximum heat transfer rate for given conditions can be written as:

$$\dot{Q}_{\text{max}} = \left(\dot{m} C_{\text{p}}\right)_{\text{min}} \Delta T_{\text{max}} \tag{19}$$

Here, $(\dot{m}C_{\text{p}})_{\text{min}}$ is the smaller one of the hot and cold fluids of the Shex where ΔT_{max} is the temperature difference between higher and lower temperatures of the streams entering the heat exchanger. For the exergy analysis, the exergy balance equation is given below [21]:

$$\dot{E}x_{\text{Q}} - \dot{E}x_{\text{W}} = \sum \dot{m}_{\text{out}} e_{\text{out}} - \sum \dot{m}_{\text{in}} e_{\text{in}} + \dot{E}x_{\text{dest}} \tag{20}$$

In above equation, $\dot{E}x$ is the exergy flow; e is the flow exergy of the stream, and $\dot{E}x_{\text{dest}}$ is the exergy destruction rate. The exergy of heat, work and flow exergy terms are defined below:

$$\dot{E}x_{\text{Q}} = \dot{Q}\left(\frac{T - T_0}{T}\right) \tag{21}$$

$$\dot{E}x_{\text{W}} = \dot{W} \tag{22}$$

$$e = (h - h_0) - T_0(s - s_0) \tag{23}$$

For the calculation of the exergy of solar, the formula defined by Ref. [22] is used:

$$\dot{E}x_{\text{solar}} = SA_{\text{a}}\left(1 + \frac{1}{3}\left(\frac{T_0}{T_{\text{sun}}}\right)^4 - \frac{4}{3}\left(\frac{T_0}{T_{\text{sun}}}\right)\right) \tag{24}$$

Finally, the energy efficiency, coefficient of performance (COP) value of absorption refrigeration system, and exergy efficiency terms are described below:

$$\eta_{en} = \frac{\dot{E}_{out}}{\dot{E}_{in}} \tag{25}$$

$$COP = \frac{\dot{Q}_{evap}}{\dot{Q}_{gen}} \tag{26}$$

$$\eta_{ex} = \frac{\dot{E}x_{out}}{\dot{E}x_{in}} \tag{27}$$

4 Results and Discussions

For the energy and exergy analyses of solar-assisted integrated power and refrigeration system, the thermodynamic properties of the working fluids are determined using EES software (Klein 2018). Energy and exergy efficiencies, refrigeration capacity, as well as the net power generated for different supercritical fluids, required heat input, and the exergy destructions are calculated using the equations given in the previous section. Since the working pressure of CO_2 is relatively high with that of the R170 and R41, the analysis is made for constant turbine inlet pressure and constant pressure ratio (r_P). The calculated power generation and refrigeration capacities are given in Fig. 2 for constant turbine inlet pressure for different fluids. As seen from the figure, the maximum power generation is achieved by R170 with a value of 32.54 kW, followed by R41 and R744. This result is because of the higher pressure ratio of R170 and R41. Also, the pressure ratios are displayed in the figure. It must be noted

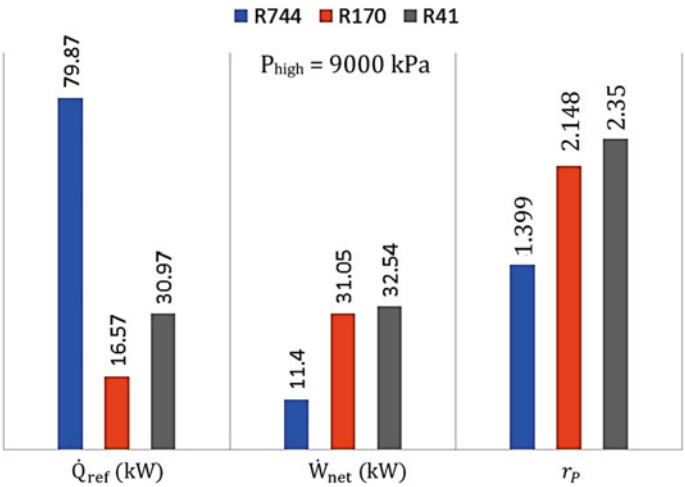

Fig. 2 Calculated refrigeration and power generation with pressure ratio for constant turbine inlet pressure

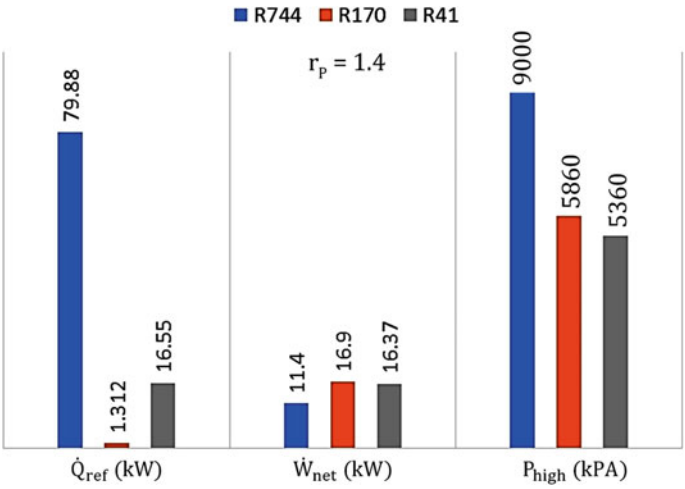

Fig. 3 Calculated refrigeration and power generation with turbine inlet pressure constant pressure ratio

that the turbine outlet pressure is the saturation pressure at condenser temperature, while inlet pressure is 9000 kPa.

For the refrigeration capacity, the integrated ORC working with R744 has the highest capacity value with 79.87 kW, while for the others, the capacities are calculated to be very low. This is mainly due to the solar energy gained by the cycles. For power generation, ORC working with R170 and R41 absorbs the major part of the solar energy with the remaining less solar heat for ARS. For R744, the power generation is low, with remaining more solar energy for ARS. This will be explained in detail next. In Fig. 3, the calculations are given for constant r_P. This means the turbine inlet pressure was calculated by multiplying condenser saturation pressure with r_P. As expected, the power generation rates decrease since the turbine inlet pressure decrease for R170 and R41. Also, the refrigeration capacities are lower than previous calculations since most of the heat energy was used for power generation. As seen from the figure, for R170, the refrigeration capacity is very close to zero. Also, the difference between the high pressure of R744 with R170 and R41 is noteworthy.

The main reason lying under the previous two results is depending on the specific heat capacity and specific volume of the fluids. In Fig. 4, the variation of these values with temperature is displayed for pressure of 9000 kPa. For all fluids, there is a bounce which is very sharp for R744 and relatively slight for the others. This is because the pressure is close to critical pressure for R744 and far for the others. After this bounce, all the lines become nearly flat. The other reason which is more meaningful is the difference between C_p values. R170 has the highest C_p followed by R41 and R744. This means the amount of energy required for heating of R170 is much more than the others, which leads to remaining less heat energy for ARS.

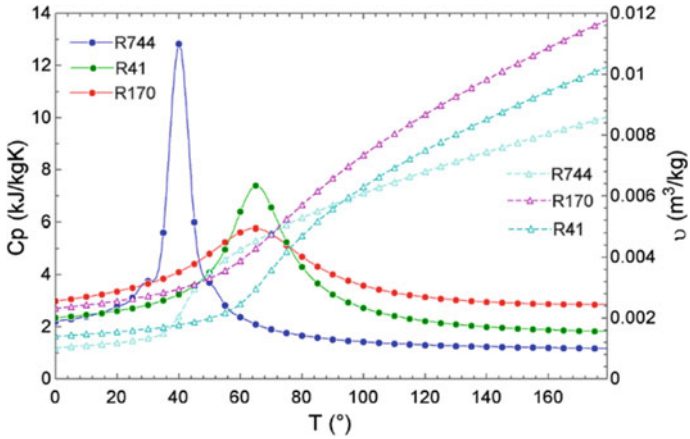

Fig. 4 Variation of specific heat and volume as a function of temperature ($P = 9000$ kPa)

Additionally, the right-hand side of Fig. 4 shows the variation of specific volumes. R170 has the highest specific volume that explains the reason for the highest power generation rate.

On the contrary to these results, R744 has the highest exergy destruction rate, followed by R170 and R41 (Fig. 5). The calculations were made for constant high pressure. It must be noted that the figure was plotted by excluding the exergy destruction rate of the solar collectors, which remains constant for all calculations. This is because the HTF and the PTSC are independent of the other cycle parameters. The collector, exergy destruction rate is 294 kW which is mainly due to the temperature

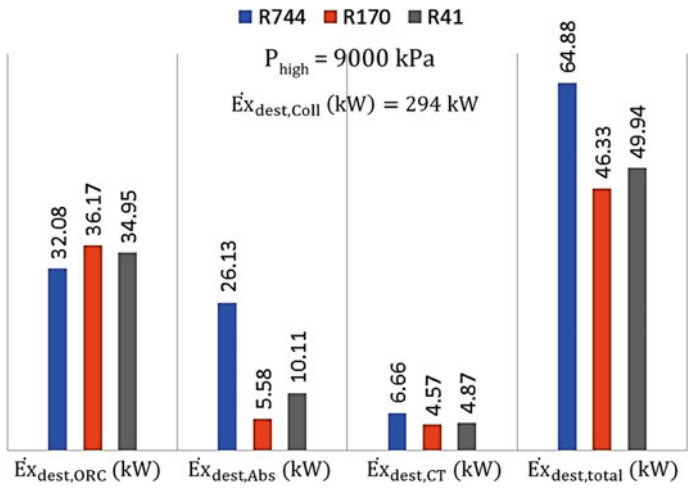

Fig. 5 Exergy destruction rates for constant turbine inlet pressure

difference between the sun and the receiver of the PTSC. The results of the individual cycle are also given in the figure. For ORC, R744 has the lowest destruction rate due to absorbing a low amount of heat for power generation, as explained before.

For the thermal processes, the exergy destruction rates mainly occur during heat transfer operations; the higher heat transfer rate causes higher exergy destruction rates. As evidence, the exergy destruction rate of ARS integrated with the R744 cycle is the highest because of much more heat energy utilization. In Fig. 6, the results are given for constant r_P. As previously declared, the power generation rated decreases for R170 and R41, which means higher exergy destruction rates.

Figures 7 and 8 show the efficiencies of the cycles for two conditions. In Fig. 7, for high pressure of 9000 kPa, the energy and the exergy efficiencies have got the same trend as for the power generation except for overall efficiency. The overall efficiency calculated here is the rate of total power generation and refrigeration to absorbed solar energy. Although cycle working with R744 has the lowest energy production rate, it has a remarkable refrigeration capacity which leads to higher overall efficiency.

In Fig. 8, the energy efficiency of ORC working with R744 is higher than the others. The reason for that is R41 and R170 cycles require more thermal energy for the power generation, as explained before, and this results in lower energy efficiency. Additionally, in Figs. 7 and 8, the COP of ARS is constant and calculated as 0.785, which is adequate for solar applications. The efficiency of the solar collector is found to be 73.15%, and it is also constant since it is not affected by the working fluid type and cycles.

For the analysis, parametrical studies were also carried out to determine the effect of working parameters on system performance. Figures 9 and 10 show the variation of net power generation and the energy efficiency of ORC with turbine inlet pressure and temperature, respectively. As expected, with the increase of turbine inlet pressure,

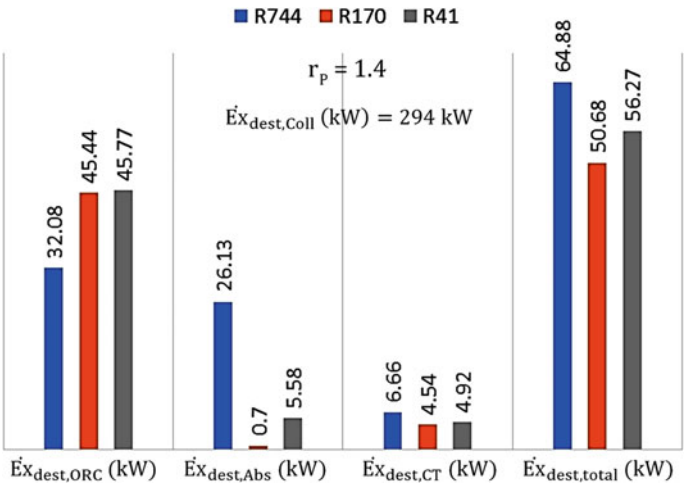

Fig. 6 Exergy destruction rates for constant pressure ratio

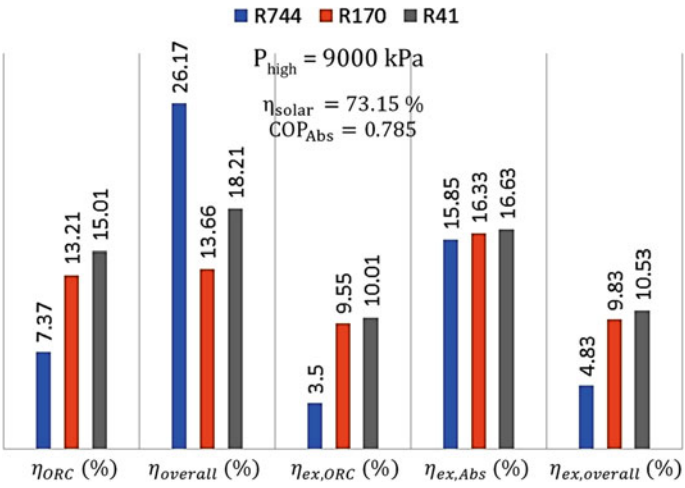

Fig. 7 Efficiencies for constant turbine inlet pressure

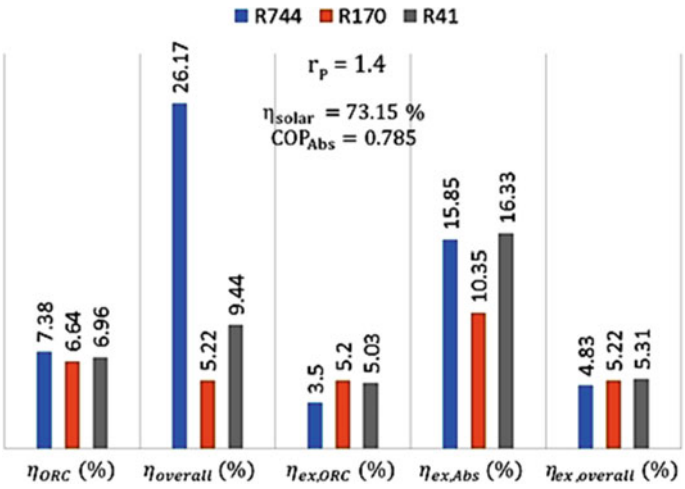

Fig. 8 Efficiencies for constant pressure ratio

power generation and energy efficiency increase for all working fluids. Also, turbine inlet temperature has got the same effect on these outputs.

The effect of the turbine inlet pressure on the exergy destruction rate and exergy efficiency of ORC is given in Fig. 11. On the contrary to power generation, with the increase of high pressure, the exergy destruction rates decrease for all supercritical working fluids. Also, from the figure, it can be seen that the lowest exergy destruction occurs in the system working with R170. The trend for the exergy efficiency is the opposite of this result, as expected. With the increasing turbine inlet pressure, exergy

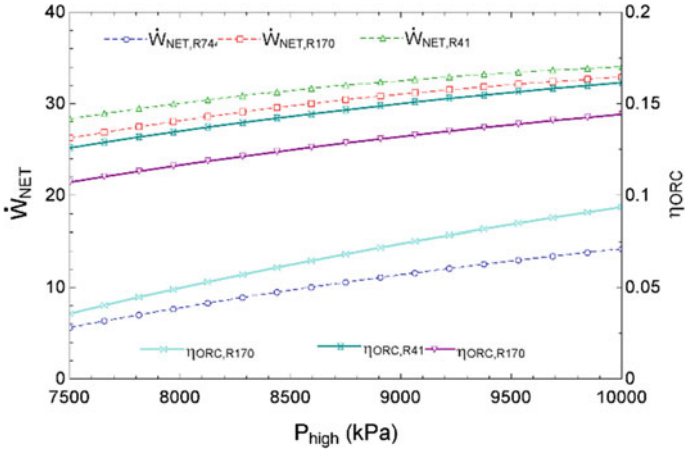

Fig. 9 Variation of power generation and energy efficiency of ORC with turbine inlet pressure

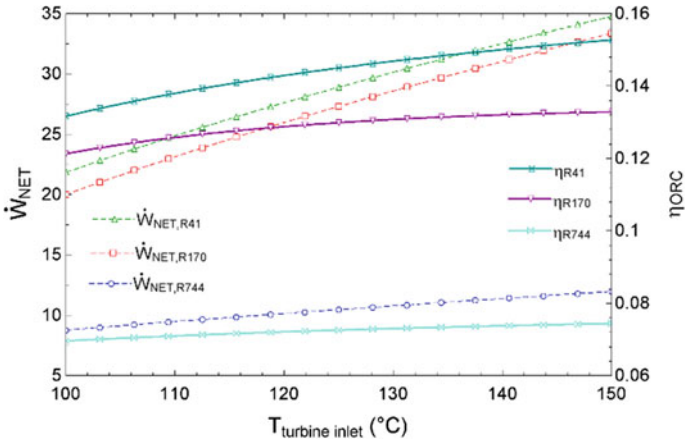

Fig. 10 Variation of power generation and energy efficiency of ORC with turbine inlet temperature

efficiency increases for all fluids. The increment ratio is slightly higher for R744 than the others.

The effect of the turbine inlet temperature is more evident than the pressure, as seen from Fig. 12. With the increase of temperature, the destruction rate decreases substantially for all fluids. The decrement ratio is higher for R170, followed by R41 and R744. The exergy efficiency acts the same as the turbine inlet temperature. The increment ratio R41 and R170 is higher than R744. This mainly depends on specific heat and the specific volume of the fluids.

Finally, a calculation was carried out for determining the necessary PTSC length and is for a given power and refrigeration duty as displayed in Fig. 13. Calculations

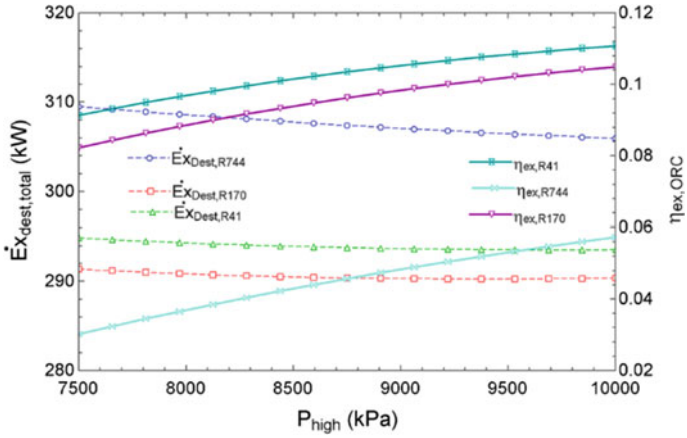

Fig. 11 Variation of exergy destruction rate and exergy efficiency of ORC with turbine inlet pressure

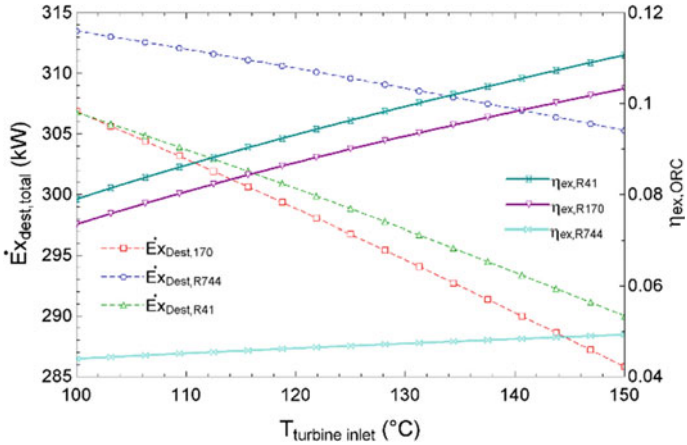

Fig. 12 Variation of exergy destruction rate and exergy efficiency of ORC with turbine inlet temperature

were made for a turbine net power generation of 50 kW for ORC and a refrigeration capacity of 50 kW for ARS. The necessary PTSC dimensions were determined for all cycles individually. As seen from the figure, an ORC working with R744 requires 265.3 m of PTSC, which corresponds to an area of 1234 m^2. For the same power generation, an ORC working with R170 requires 148.1 m PTSC, while it is 130.3 m for R41. Also, it must be noted that the calculations were made for a turbine inlet pressure of 9000 kPa.

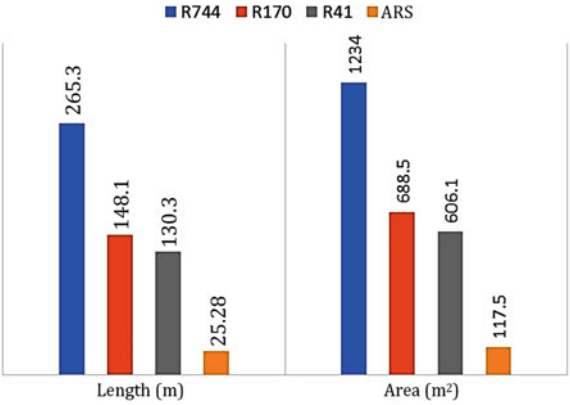

Fig. 13 Required PTSC length and area for 50 kW net power generation or refrigeration

5 Conclusions

Comprehensive energy and exergy analyses were carried out to evaluate the performance of PTSC-assisted ORC integrated with absorption refrigeration. The calculations were made for three different working fluids: R744, R170, and R41. According to the results, the followings were concluded:

- ORC working with R41 has the highest power generation rate with 32.54 kW for a turbine inlet pressure of 9000 kPa.
- For the constant pressure ratio, R41 again has the lowest net power generation of 16.37 kW, while the turbine inlet pressure of the cycle is 5360 kPa.
- The maximum refrigeration capacity for ARS is obtained for the integrated system working with R744 with a value of 79.88 kW due to higher remaining solar energy after vaporizer.
- According to the exergy analysis, R744-integrated system has the highest destruction rates for both cases, constant pressure and constant pressure ratio.
- Turbine inlet pressure and temperature have remarkable effects on system performances for all working fluids.
- The best working fluid for both power generation and refrigeration is R41 even though with relatively lower refrigeration capacity. If the refrigeration capacity is more important than power generation, the system with R744 can be preferable due to its very high refrigeration capacity.
- The minimum PTSC length for a power generation of 50 kW is calculated for the cycle using R41 with 130.3 m.
- The specific heat capacity and specific volume of the working fluid are very important for the power cycles as well as the other parameters.

References

1. Zhang XR, Yamaguchi H, Fujima F, Enomoto M, Sawada N (2005) A Feasibility study of CO_2-based Rankine cycle powered by solar energy. JSME Int J Ser B 48(3):540–547
2. Zhang XR, Yamaguchi H, Uneno D, Fujima K, Enomoto M, Sawada N (2006) Analysis of a novel solar energy-powered Rankine cycle for combined power and heat generation using supercritical carbon dioxide. Renewable Energy 31:1839–1854
3. Singh H, Mishra RS (2018) Performance analysis of solar parabolic trough collectors driven combined supercritical CO_2 and organic Rankine cycle. Eng Sci Technol Int J 21(3):451–464
4. Al-Sulaiman FA (2013) Energy and sizing analyses of parabolic trough solar collector integrated with steam and binary vapor cycles. Energy 58:561–570
5. Mocarski S, Gozdur AB (2015) Selected aspects of operation of supercritical (transcritical) organic Rankine cycle. Arch Thermodyn 36(2):85–103
6. Yamaguchi H, Zhang XR, Fujima K, Enomoto M, Sawada N (2006) Solar energy powered Rankine cycle using supercritical CO_2. Appl Therm Eng 26:2345–2354
7. Garg P, Srinivasan K, Dutta P, Kumar P (2014) Comparison of CO_2 and steam in transcritical Rankine cycles for concentrated solar power. Energy Procedia 49:1138–1146
8. Sarkar S (2015) Review and future trends of supercritical CO2 Rankine cycle for low-grade heat conversion. Renew Sustain Energy Rev 48:434–451
9. Wang D, Lu Y, Tao L (2017) Thermodynamic analysis of CO2 blends with R41 as an azeotropy refrigerant applied in small refrigerated cabinet and heat pump water heater. Appl Therm Eng 125:1490–1500
10. Nemati A, Mohseni R, Yari M (2018) A comprehensive comparison between CO_2 and Ethane as a refrigerant in a two-stage ejector-expansion transcritical refrigeration cycle integrated with an organic Rankine cycle (ORC). J Supercrit Fluids 133(1):494–502
11. Liao J, Zheng Q (2014) Thermodynamic analysis of low-temperature power generation transcritical rankine cycle with R41 And CO2. In: Proceedings of ASME turbo expo 2014: turbine technical conference and exposition GT2014
12. Khaliq A, Kumar R, Mokheimer EMA (2018) Investigation on a solar thermal power and ejector-absorption refrigeration system based on first and second law analyses. Energy 164:1030–1043
13. Crepinsek Z, Goricanec D, Krope J (2009) Comparison of the performances of absorption refrigeration cycles. WSEAS Trans Heat Mass Transfer 3(4):65–76
14. Fathi R, Ouaski S (2001) Performance of a Solar LiBr—water absorption refrigerating systems. Rev Energ Ren Journées de Thermique 73–78
15. Kizilkan O (2018) Exergetic performance assessment of solar driven combined CO2 power and refrigeration system. Int J Exergy 27(2):147–164
16. Babatunde AF, Sunday OO (2018) A review of working fluids for organic rankine cycle (ORC) applications. IOP Conf Ser Mater Sci Eng 413
17. Shengjun Z, Huaixin W, Tao G (2011) Performance comparison and parametric optimization of subcritical organic Rankine cycle (ORC) and transcritical power cycle system for low-temperature geothermal power generation. Appl Energy 88(8):2740–2754
18. Kalogirou SA (2009) Solar energy engineering: processes and systems. Academic Press, Oxford
19. Cengel YA, Boles MA (2006) Thermodynamics: an engineering approach. McGraw-Hill, New York, USA
20. Herold KE, Radermacher R, Klein SA (2016) Absorption Chillers and heat pumps. CRC Press, Boca Raton, FL, p 346
21. Dincer I, Rosen MA (2013) Exergy: energy, environment and sustainable development. Elsevier Science, p 576
22. Petela R (2005) Exergy analysis of the solar cylindrical-parabolic cooker. Sol Energy 79:221–233